Journal for Multiscale Computational Engineering, 10 (2): 171–188 (2012)

IN VITRO/IN SILICO CHARACTERIZATION OF ACTIVE AND PASSIVE STRESSES IN CARDIAC MUSCLE

Markus Böl,[1] Oscar J. Abilez,[2] Ahmed N. Assar,[2] Christopher K. Zarins,[2] & Ellen Kuhl[3,*]

[1]*Department of Mechanical Engineering, TU Braunschweig, 38106 Braunschweig, Germany*

[2]*Department of Surgery, Stanford University, Stanford, CA 94305*

[3]*Departments of Mechanical Engineering, Bioengineering, and Cardiothoracic Surgery, Stanford University, Stanford, CA 94305*

[*] Address all correspondence to Ellen Kuhl, E-mail: ekuhl@stanford.edu

We propose a novel, robust, and easily reproducible, in vitro/in silico model system to characterize active and passive stresses in electroactive cardiac muscle using a hybrid experimental/computational approach. We explore active and passive stresses in healthy explanted heart slices in vitro, design a virtual test bed to simulate the in vitro measured stresses in silico, and predict altered active force generation in infarcted hearts in silico. For the in vitro model, explanted rat heart tissue slices are mounted on a force transducer and stimulated electrically through biphasic pulses. Isometric forces are recorded and translated into active circumferential stress. For the in silico model, stresses are additively decomposed into passive and active contributions, with the latter being related to the measured isometric force. A hierarchical finite element model for cardiac muscle tissue is developed based on passive tetrahedral unit cells, representing a network of interconnected polymeric chains, and active trusses, representing the contracting muscle fibers. First, we calibrate the model against our experiments with healthy explanted rat heart slices. Then, we predict acute and chronic alterations in active stress generation in infarcted hearts. We virtually explore isometric forces generation for different infarct area fractions and infarct locations. This approach has the potential to precisely quantify global loss of cardiac function for a given infarct area fraction.

KEY WORDS: *chain network models, multiscale modeling, cardiac muscle, electroactive materials, finite element method*

1. INTRODUCTION

Almost 80 million American adults have one or more types of cardiovascular disease. Of these, 7.2 million have had a myocardial infarction, with 1.6 million new or recurring cases each year; approximately one-third of these cases are terminal. Myocardial infarction is the result of a loss of myocardial blood supply (Kumar et al., 2005). Acutely, the functional units of the myocardium, the cardiomyocytes, lose their contractile property and die; chronically, these dead cardiomyocytes are replaced by stiff scar tissue (Göktepe et al., 2010a,b).

The capacity for self-regeneration in adult tissues such as the heart is severely limited. Recently, stem cell therapies have emerged as a promising methodology for cardiac repair (Abilez et al., 2006a,b; Wollert et al., 2004; Zimmermann et al., 2006). However, to predict and improve the potential of stem cell therapies, it is essential to fully understand the interplay between active and passive stresses in healthy and diseased hearts (Itoh et al., 2009; Tsamis et al., 2011). In this paper, we suggest a computational model for force generation in healthy and infarcted tissue following the common approach to additively decompose the overall stresses in passive and active contributions (Costa et al., 2001; Göktepe and Kuhl, 2010; Hunter et al., 1998). Passive tissue properties have been studied intensely in the

1543–1649/12/$35.00

past (Ehret and Itskov, 2009; Schmid et al., 2008). For cardiac tissue, they are typically determined through *in vitro* experiments of explanted tissue blocks (Dokos et al., 2002; Omens et al., 1993). Far less is known about the active tissue properties. Most available data sets on active stress generation are based on isolated skeletal muscle (Gordon et al., 1966), papillary muscle (Brooks and Conrad, 1999; Capasso et al., 1986), or trabeculae carneae (Mulieri et al., 1989), rather than ventricular cardiac muscle, presumably because skeletal muscle is more structured and its fibers can be isolated more easily. Recently, explanted heart slices have been recognized as a valuable, robust, long-term, *in vitro* model system to study active force generation in healthy and diseased cardiac tissue (Habeler et al., 2009; Pillekamp et al., 2005).

Active contraction in muscular tissue can be studied *in vitro* in different test setups, isotonic and isometric (Hunter et al., 1998). In isotonic contraction, one end of the muscle is fixed while the other end is free to move as the muscle contracts against a constant force. In isometric contraction, both muscle ends are fixed and muscle contraction generates contractile force. Following the latter approach, we suggest an experimental setup in which fresh explanted tissue slices are mounted at both ends (Pillekamp et al., 2005), and circumferential isometric contraction is recorded on electrical stimulation (Halbach et al., 2006). This test setup has the following fundamental advantages over testing single isolated muscle fibers: (i) slices are easier to couple to force transducers than individual fibers; (ii) tissue slice tests do not rule out the effects of intercellular cross-talk; and (iii) the anatomic and functional integrity of the tissue slice remains intact over long periods post explantation (Pillekamp et al., 2007b). Heart slices have been reported to remain viable in long-term culture, displaying spontaneous contraction up to three months (Habeler et al., 2009).

Motivated by the success of these heart-slice experiments, we design a computational test bed to virtually probe the role of passive and active cardiac stresses in healthy and diseased hearts. In contrast to the recently proposed phenomenological models for passive cardiac tissue (Göktepe et al., 2011; Holzapfel and Ogden, 2009; Schmid et al., 2006, 2009), we pursue an approach in which the passive material response is characterized by means of discrete representative volume elements in the form of tetrahedra. These elements have originally been developed for rubberlike materials (Böl and Reese, 2006), and are now modified for networks of biopolymers in muscular tissue (Böl and Reese, 2007, 2008). The characteristic microstructure of the polymeric tissue network is incorporated through the statistical mechanics of long chain molecules (Flory, 1969; Treloar, 1975) represented discretely at the six edges of each tetrahedral element. In the original rubber model, the individual chains are characterized through freely jointed chains following Langevin statistics. Here, we model the individual chains as wormlike chains with an initial stiffness characterized through the persistence length (Bustamante et al., 1994; Kratky and Porod, 1949; Kuhl et al., 2005, 2006; Kuhl and Holzapfel, 2007). In addition to the energy of the six wormlike chain bundles on the tetrahedral edges, each tetrahedral energy accounts for an incompressible ground substance through a phenomenological volumetric free energy term (Böl and Reese, 2007; Böl, 2012).

Active contractility is attributed exclusively to the cardiomyocyte fibers (Böl and Reese, 2009). According to the sliding filament theory, active cardiomyocyte force is generated by thick myosin filaments sliding along thin filaments of actin (Bers, 2001; Huxley and Hanson, 1954; Opie, 2003). The resulting force-length relation is characterized through an optimal stretch at which cardiomyocytes generate maximum force (Allen et al., 1974; Bers, 2001; Hunter et al., 1998). In the living heart, the fiber stretch can be related to the diastolic volume, while the active fiber force can be related to the ventricular pressure. Starling's law of the heart states that the ventricular pressure, or the active fiber force, is proportional to the diastolic volume, or the cardiomyocyte stretch (Berne and Levy, 2001; Ganong, 2003). In the computational model, the resulting characteristic one-dimensional force-length relation is accounted for by specially designed actively contracting truss elements. Provided the exact muscle fiber directions are known, e.g., from diffusion tensor MRI, these trusses can simply be aligned with the experimentally measured muscle fiber directions. Here, for the sake of simplicity, we assume that the cardiac muscle fibers are primarily oriented in the circumferential direction.

This paper is organized as follows. In Section 2, we describe the tissue slice preparation and the experimental setup to measure isometric cardiac muscle forces. Section 3 summarizes the constitutive equations for passive and active stresses. Section 4 documents the features of the proposed approach by means of computational examples. Its first part illustrates the calibration of the simulation tool for slices of healthy hearts, whereas the second part shows the prediction of active stress alterations in slices of diseased hearts. The paper concludes with a brief discussion of potential future research directions in Section 5.

2. IN VITRO MEASUREMENT OF ISOMERIC FORCES

In this section, we illustrate the experimental procedure to measure active cardiac contraction in an isometric setting.

2.1 Heart Tissue Preparation

All care and treatment of animals were in accordance with the National Institutes of Health Policy on Humane Care and Use of Laboratory Animals and were subjected to prior approval by the Stanford Administrative Panel on Laboratory Animal Care (APLAC). Young male Sprague-Dawley rats (125 g, 9–17 days old) were anesthetized with sodium pentobarbital (50 mg/kg) intraperitoneally. A left lateral thoracotomy was performed to expose the beating heart, the pericardium was incised, and the heart was removed by transecting the vena cavae, the pulmonary arteries and veins, and the aortic root. The heart was immediately transferred to prewarmed Krebs-Henseleit buffer and then cut in 2 mm axial slices by using a stainless steel tissue slicer (Harvard Apparatus, Holliston, MA); see Fig. 1. The slices resulted in ring-shaped tissue comprising the right and left ventricles.

2.2 Electrical Stimulation and Isometric Force Measurements

The isometric force test apparatus consisted of a force transducer (Model 724480, Harvard Apparatus, Holliston, MA) with two selectable ranges, 0–0.005 N and 0–0.05 N, and accuracy of $\pm 1\%$; a micrometer positioning system (Model 47700, World Precision Instruments (WPI), Sarasota, FL); and a tissue holder with two 5 mm flexible platinum stimulation electrodes (Model 47050, WPI, Sarasota, FL) positioned next to two L-shaped stainless steel holders (see Figs. 2 and 3).

During tissue stimulation, the test apparatus was immersed in Krebs-Henseleit buffer with 2.5 mM Ca^{2+}. The media was constantly circulated via a variable flow mini-pump (Model 57951-016, VWR, West Chester, PA). The media bath was continuously bubbled with 95% O_2 and 5% CO_2 and maintained at 37°C. An electrical field stimulator (Model SIU-102, Warner Instruments, Hamden, CT) was used to pace tissue by applying biphasic pulses (1.0 Hz, 10 ms pulse width, 20 V peak-peak) across the titanium electrodes spaced approximately 1-2 cm apart across the tissue. Analog voltage signals from the force transducer were transferred to a USB data acquisition device (USB-6009, National Instruments (NI), Austin, TX) and displayed, analyzed, and recorded with LabView 8.2 software (NI, Austin, TX).

2.3 Heart Force Acquisition

Two-millimeter-thick, ring-shaped axial heart slices were mounted around the two L-shaped holders of the force test apparatus and were allowed to equilibrate with oxygenated KHB for 30 min at 37°C. Tissue preparations were gradually stretched stepwise, by increments of 0.05 mm increased every 2 min. The total displacement of 1 mm corresponded to an axial tissue stretch of $\sim 15\%$. Electrical field stimulation of 1 Hz was applied to the tissue at all

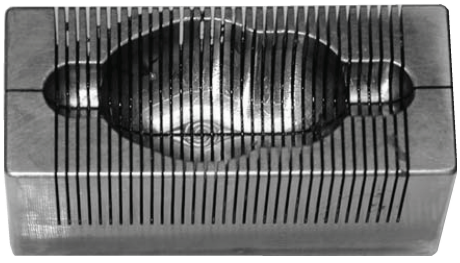

FIG. 1: Rodent heart slicer for ventricular axial slicing. The slicer allows for precise sectioning of reproducible tissue samples with thickness increments as narrow as 1 mm to analyze explanted healthy and infarcted hearts. The tissue slices used in the present study are 2 mm thick.

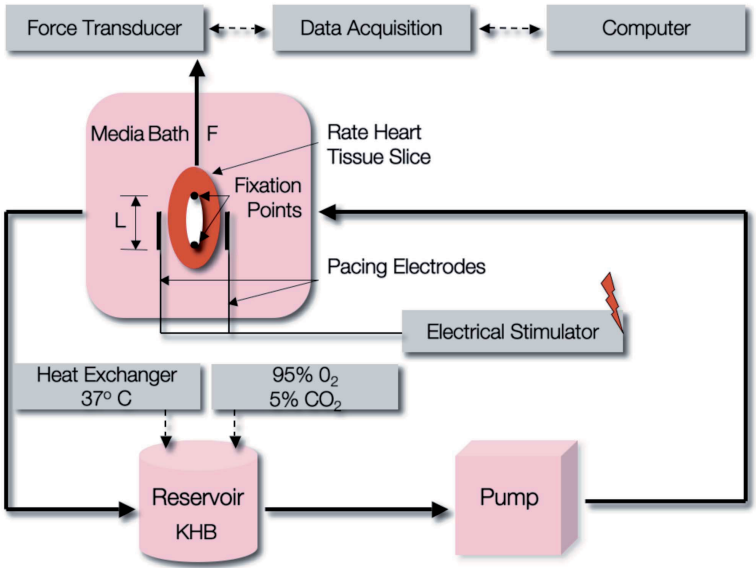

FIG. 2: Schematic of isometric force test apparatus. Tissue slices are mounted on the tissue holder in a media bath and stimulated electrically by applying biphasic pulses. Analog voltage signals upon tissue contraction are recorded through a force transducer and converted into active tissue force.

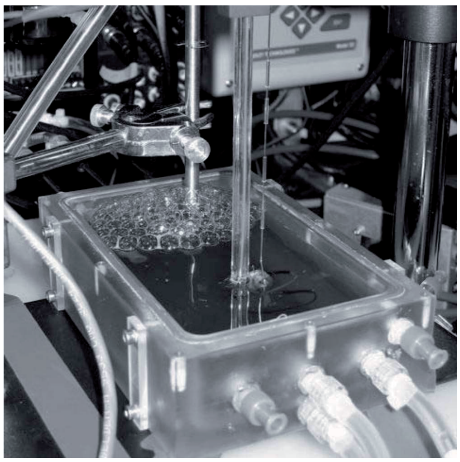

FIG. 3: Photograph of isometric force test apparatus. Tissue slices are mounted on the tissue holder in a media bath and stimulated electrically by applying biphasic pulses. Analog voltage signals upon tissue contraction are recorded through a force transducer and converted into active tissue force.

given stretches, and the resulting isometric forces were sampled at 25 Hz resulting in 25 data points per beat. The recorded total force $F = F^{\mathrm{pas}} + F^{\mathrm{act}}$ for 20 load increments applied over a period of 40 min is displayed in Fig. 4.

For each preload level, we generated the upper and lower envelopes of the force readings and interpreted their horizontal asymptotes as the total force $F = F^{\mathrm{pas}} + F^{\mathrm{act}}$ and passive force F^{pas}, respectively. This allowed us to minimize viscous effects without having to wait for full convergence to a stable plateau. Figure 5 documents a representative force versus time plot for load level 7 at a preload of 4.5% stretch. The red line, the upper envelope,

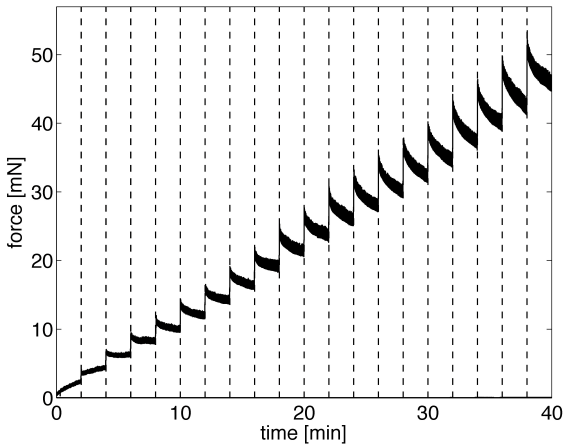

FIG. 4: *In vitro* measured isometric contraction of explanted rat heart slice stimulated at 1 Hz at different preload levels. Total force $F = F^{\mathrm{pas}} + F^{\mathrm{act}}$ is plotted versus time. Preload is increased discontinuously by 0.05 mm every 2 min, and then held constant to minimize viscous effects. Maximum preload level of 1 mm after 20 load increments (i.e., after 40 min), corresponds to a stretch of $\sim 15\%$.

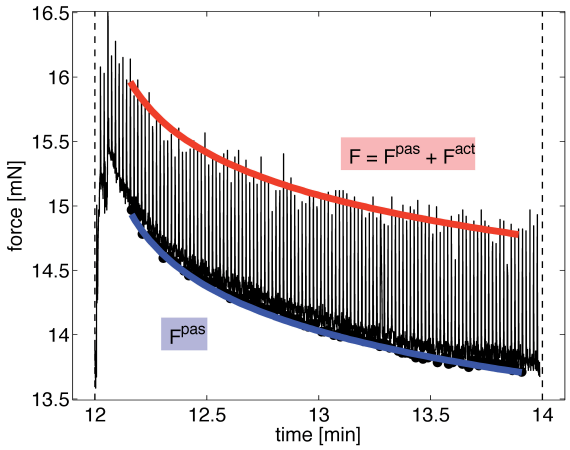

FIG. 5: *In vitro* measured isometric contraction of explanted rat heart slice stimulated at 1 Hz. Representative force versus time plot for load level 7 corresponding to a preload level of 0.30 mm (i.e., $\sim 4.5\%$ stretch). Red and blue lines illustrate upper and lower envelopes of recorded force data for 100 beats. Horizontal tangents of both envelopes are interpreted as total force $F = F^{\mathrm{pas}} + F^{\mathrm{act}}$ and passive force F^{pas}, respectively.

corresponds to the total force. The blue line, the lower envelope, corresponds to the passive force. For this load level, the converged total force and the corresponding passive force were calculated to $F = F^{\mathrm{pas}} + F^{\mathrm{act}} = 12.88$ mN and $F^{\mathrm{pas}} = 11.86$ mN, respectively.

The resulting converged forces for all 20 preload levels were interpreted as the discrete representation of the *in vitro* measured total and passive forces. Figure 6 shows the passive forces F^{pas} as discrete circles and the active forces F^{act} as discrete squares. The depicted curves correspond to the smooth continuous representation of passive and active forces obtained from a least-squares fit. In Section 3, these curves will be used to calibrate the material parameters of the constitutive model.

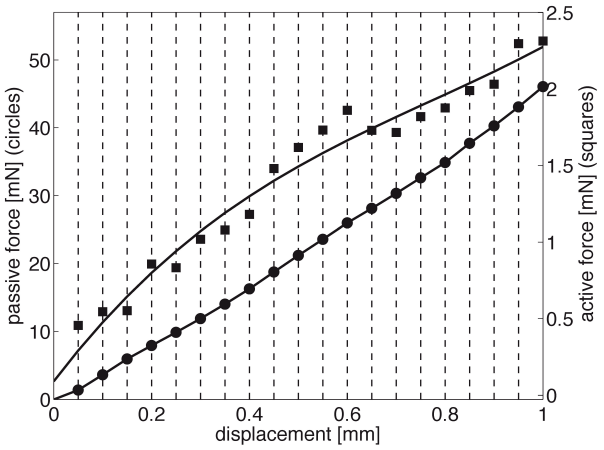

FIG. 6: *In vitro* measured isometric contraction of rat heart slice for different preload levels. Converged passive force F^{pas} (circles) and the converged active force F^{act} (squares) are shown for each load step of 0.05 mm. Discrete circles and squares represent the *in vitro* measured values, continuous lines indicate the least-squares fit of the *in vitro* measurements. At maximum preload of $\sim$15% stretch, the passive force F^{pas} is $\sim$20 times larger than the active force F^{act}.

3. IN SILICO MODEL OF ACTIVE AND PASSIVE STRESSES

In this section, we summarize the constitutive equations for actively contracting cardiac muscle tissue. To characterize the mechanical properties of the tissue slices analyzed in Section 2, we suggest an additive decomposition of the overall tissue stress $\boldsymbol{\sigma}$ into an active and a passive part,

$$\boldsymbol{\sigma} = \boldsymbol{\sigma}^{\mathrm{pas}} + \boldsymbol{\sigma}^{\mathrm{act}} \tag{1}$$

where $\boldsymbol{\sigma}$ denotes the Cauchy stress acting on the deformed configuration. Because we will calibrate our model in terms of the converged active and passive stresses, we can neglect time-dependent rate effects. The passive stress $\boldsymbol{\sigma}^{\mathrm{pas}}(\boldsymbol{F})$ is therefore characterized exclusively in terms of the deformation gradient $\boldsymbol{F} = \nabla\,\boldsymbol{\varphi}$, where $\boldsymbol{\varphi}$ is the deformation map, neglecting viscous effects. The active stress $\boldsymbol{\sigma}^{\mathrm{act}}(\boldsymbol{F}, \boldsymbol{n}^{\mathrm{fib}})$ is caused by the active cardiomyocyte force acting along the cardiomyocyte direction $\boldsymbol{n}^{\mathrm{fib}}$, neglecting force-velocity effects. According to Starling's law of the heart, the active cardiomyocyte force can be related to the degree of ventricular filling represented locally through the deformation gradient $\boldsymbol{F}$, or more precisely, through the cardiomyocyte stretch $\lambda^{\mathrm{fib}} = \sqrt{\boldsymbol{n}^{\mathrm{fib}} \cdot \boldsymbol{F}^T \cdot \boldsymbol{F} \cdot \boldsymbol{n}^{\mathrm{fib}}}$.

3.1 Passive Stress $\boldsymbol{\sigma}^{\mathrm{pas}}$

In general, the passive myocardial response is characterized by large deformations, a nonlinear stress-strain relation, and a quasi-incompressibility. We propose to describe this behavior through an approach adopted from statistical mechanics of long chain molecules originally developed for rubberlike materials (Böl and Reese, 2006). In this approach, the characteristic cardiac microstructure is modeled through a discrete representative volume element based on a four-noded finite element unit cell. This cell consists of one tetrahedral element and six representative truss elements lying on each edge of the tetrahedron. The Helmholtz free energy of one unit cell then includes a contribution W^{tet} from the tetrahedral element itself and a contribution W_j^{trs} from each of the truss elements on its $j = 1, .., 6$ edges

$$W^{\mathrm{pas}} = W^{\mathrm{tet}} + \sum_{j=1}^{6} W_j^{\mathrm{trs}} \tag{2}$$

The passive Cauchy stress $\boldsymbol{\sigma}^{\mathrm{pas}}$ then follows from thermodynamical considerations and can be expressed as the push forward of the second Piola Kirchhoff stress $2\partial W^{\mathrm{pas}}/\partial \boldsymbol{C}$,

$$\boldsymbol{\sigma}^{\mathrm{pas}} = \frac{1}{J}\,\boldsymbol{F}\cdot 2\,\frac{\partial W^{\mathrm{pas}}}{\partial \boldsymbol{C}}\cdot \boldsymbol{F}^{T} \tag{3}$$

where $J = \det \boldsymbol{F}$ denotes the determinant of the macroscopic deformation gradient $\boldsymbol{F}$, and $\boldsymbol{C} = \boldsymbol{F}^{T}\cdot\boldsymbol{F}$ is the right Cauchy Green deformation tensor. The tetrahedral contribution

$$W^{\mathrm{tet}} = \frac{1}{4}\,K\,\left[J^2 - 1 - 2\ln J\right] \tag{4}$$

which is weighted by the bulk modulus K describes the volumetric behavior of the unit cell. Giving the structure its volumetric stiffness, it is primarily attributed to the fluid part of the tetrahedral muscle tissue. We suggest that the passive ventricular tissue can be considered as a three-dimensional network composed of a large number of collagen fibers that are collectively represented as six trusses per unit cell. The micromechanical material behavior of each fiber bundle j is characterized by the second term of Eq. (2),

$$W^{\mathrm{trs}} = \frac{1}{A_0\,L_0}\,\nu^{\mathrm{col}}\,W^{\mathrm{col}} \tag{5}$$

where A_0 and L_0 denote the cross section and length of the undeformed truss element, respectively, and $\nu^{\mathrm{col}} = N^{\mathrm{col}}/N^{\mathrm{trs}}$ defines the number of collagen fibers N^{col} per truss element N^{trs} (Böl and Reese, 2006). The energy of one collagen fiber

$$W^{\mathrm{col}} = \frac{k\theta}{4\,A^{\mathrm{mod}}}\left[\frac{2(\lambda^{\mathrm{col}})^2}{\sqrt{n}} + \frac{\sqrt{n}}{[1-\lambda^{\mathrm{col}}/\sqrt{n}]} - \lambda^{\mathrm{col}}\right] \tag{6}$$

is motivated by the classical wormlike chain model (Kratky and Porod, 1949). One fiber represents a long molecular chain with n bonds of fixed bond length l. Collagen fibers are distinguished through a smooth curvature whose direction changes randomly, but in a continuous manner. The force-length behavior of a single collagen fiber then follows straightforwardly as

$$F^{\mathrm{col}} = \frac{\partial W^{\mathrm{col}}}{\partial \lambda^{\mathrm{col}}} = \frac{k^{\mathrm{b}}\theta}{4A^{\mathrm{mod}}}\left[\frac{4\lambda^{\mathrm{col}}}{\sqrt{n}} + \frac{1}{[1-[\lambda^{\mathrm{col}}/\sqrt{n}]^2} - 1\right] \tag{7}$$

In the present approach, we use a modified persistence length $A^{\mathrm{mod}} = A/l$, which describes the ratio between the classical persistence length A and the bond length l of the fiber. Equations (6) and (7) depend on two physical parameters, namely, the Boltzmann's constant $k^{\mathrm{b}} = 1.3810\times 10^{-20}$ Nmm/K and the absolute temperature θ. In the case of living tissue, we suggest $\theta = 310$ K, i.e., $\theta = 37°$C. The distinguished feature of this discrete micromechanically motivated model is its definition of the collagen fiber stretch

$$\lambda^{\mathrm{col}} = \frac{r}{r_0} = \frac{L}{L_0} \tag{8}$$

Herein, r and r_0 denote the end-to-end length of the fiber in the deformed and undeformed state, whereas L and L_0 denote the deformed and undeformed macroscopic truss lengths, respectively.

Remark 1: *Note that the model parameter L_0 does not correlate with the length of the collagen fiber bundles. The computational efficiency of the present approach could not compete with classical continuum-based finite element computations if the mesh density would be linked to the geometry of the microstructure. An inherent advantage of the proposed framework is that the two relevant microstructural length scales L_0 and A_0 cancel out when embedded into a macroscopic finite element algorithm (Böl and Reese, 2006).*

Remark 2: *In contrast to the classical wormlike chain model, we introduce the discrete locking stretch*

$$\lambda^{\mathrm{loc}} = \frac{r^{\mathrm{loc}}}{r_0} = \frac{n\,l}{\sqrt{n}\,l} = \sqrt{n} \tag{9}$$

as the ratio between the countour length, i.e., the maximum possible end-to-end length $r^{\mathrm{loc}} = n\,l$*, and the undeformed end-to-end length* $r_0 = \sqrt{n}\,l$*. Accordingly, the locking stretch* λ^{loc} *scales linearly with the square root of the number of links per fiber* $\sqrt{n}$*.*

3.2 Active Stress $\boldsymbol{\sigma}^{\mathrm{act}}$

The unique feature of cardiac muscle is its ability to actively contract in response to an electrical signal. We incorporate active contraction through discrete representative truss elements oriented along the muscle fiber direction $\boldsymbol{n}^{\mathrm{fib}}$, generating an active overall stress $\boldsymbol{\sigma}^{\mathrm{act}}$

$$\boldsymbol{\sigma}^{\mathrm{act}} = F^{\mathrm{act}} \boldsymbol{n}^{\mathrm{fib}} \otimes \boldsymbol{n}^{\mathrm{fib}} \tag{10}$$

According to Starling's law of the heart, the active cardiomyocyte force F^{act} can be related to the degree of ventricular filling represented locally through the deformation gradient $\boldsymbol{F}$, or, more precisely, through the cardiomyocyte stretch $\lambda^{\mathrm{fib}} = \sqrt{\boldsymbol{n}^{\mathrm{fib}} \cdot \boldsymbol{F}^{\mathrm{t}} \cdot \boldsymbol{F} \cdot \boldsymbol{n}^{\mathrm{fib}}}$. The magnitude of the active stress is determined through the active force F^{act},

$$F^{\mathrm{act}}(\lambda^{\mathrm{fib}}) = \nu^{\mathrm{fib}}\, f_\lambda\,(\lambda^{\mathrm{fib}}) \tag{11}$$

which follows from the force-length relation $f_\lambda\,(\lambda^{\mathrm{fib}})$ scaled by the fiber density $\nu^{\mathrm{fib}} = N^{\mathrm{fib}} \,/\, N^{\mathrm{trs}}$, i.e., the number of fibers N^{fib} per truss element N^{trs}. Motivated by the experimental findings documented in Fig. 6, we make the following three-parameter ansatz for the force-length relation.

$$f_\lambda = f_0 + k\,[\,1 - \exp\,(\,-\eta\,\lambda^{\mathrm{fib}})\,] \tag{12}$$

The active forces thus depend on the active force in the unstretched state f_0, and on the parameters η and k. The force-length relation for $f_0 = 0\,\mathrm{mN}$, fixed η, and varying k is depicted in Fig. 7. The active contractile force of both skeletal and cardiac muscles strongly depends on the cardiomyocyte stretch λ^{fib}, which has a direct impact on the overlap between actin and myosin filaments (Allen et al., 1974; Gordon et al., 1966). In contrast to skeletal muscle, however, the active force-length relation for cardiac muscles converges to a horizontal plateau as the fiber stretch tends to infinity rather than decreasing to zero (Bers, 2001).

Remark 3: *It is virtually impossible to discretize each muscle fiber by only one truss element. In the present approach, each truss element is a discrete representation of* ν^{fib} *cardiac muscle fibers as indicated in Eq. (11).*

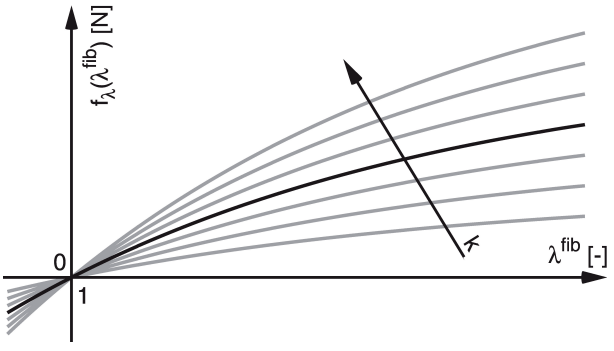

FIG. 7: Force-length relation of active cardiac muscle based on a three-parameter ansatz. Increasing the parameter k increases the steepness of the curve (see arrow). Increasing f_0 shifts the curve upward and increasing η increases the curvature (not shown).

Remark 4: *The active contractile force of both skeletal and cardiac muscles depends on the overlap between actin and myosin filaments (Allen et al., 1974; Gordon et al., 1966). However, the active force-length relation for cardiac muscle (Bers, 2001) rises more steeply than the one for skeletal muscle (Siebert et al., 2008). In cardiac muscle, the macroscopic counterpart of the force-length relation is known as Starling's law of the heart.*

4. RESULTS

In this section, we demonstrate the features of the proposed hybrid *in vitro/in silico* approach. First, we calibrate the model against our experiments based on healthy explanted rat heart slices. Then, we predict acute and chronic alterations in active force generation in infarcted hearts. We explore isometric forces generation for different infarct area fractions and infarct locations.

4.1 Baseline Isometric Force Generation in Healthy Cardiac Muscle

To calibrate our model parameters, we first explore the response of healthy slices of the heart. Figure 8 illustrates a representative 2 mm thick slice of an explanted rat heart. Its left and right ventricular geometry are used to generate a finite element model of 8013 linear tetrahedral elements. In a first approximation, cardiac muscle fibers are assumed to be oriented primarily in the circumferential direction. Mounting the heart slice to the force transducer induces a mounting stretch of 12.5%, as indicated in Fig. 9. This mounting stretch is applied in an initialization step to generate the mounted geometry from the initially unloaded heart slice. Electrical stimulation is simulated by assuming a homogeneous electric field throughout the tissue bath, inducing a cardiomyocyte contraction through the influx of sodium and calcium ions and relaxation through efflux of potassium ions (Göktepe and Kuhl, 2009; Kotikanyadanam et al., 2010). In response, the tissue slice generates an active force in the circumferential direction, which is translated into a uniaxial contraction F^{exp} measured along the mounting direction. Matching the measured passive force, we first calibrate the passive elastic material parameters $\nu^{\text{col}} = 6.75 \times 10^6$, $A^{\text{mod}} = 1.0$, $n = 9.5$, $N^{\text{col}} = 2.47 \times 10^9$ mm^{-3}, and $K = 10^7$ N/mm^2. Figure 10 illustrates the mounted slice (left) and the deformed slice under the action of passive forces (middle). Figure 11 shows the comparison between the *in vitro* measured passive forces displayed as solid lines and the corresponding *in silico* predicted passive forces displayed as circles. Next, we perform a second finite element analysis to match the active forces and calibrate the active material parameters $\nu^{\text{fib}} = 12.9$, N^{fib} = 44.1 mm^{-2}, $f_0 = 1.0 \times 10^{-4}$ mN, $k = 3.0 \times 10^{-4}$ mN, and $\eta = 0.8$. Figure 10 illustrates the deformed slice under the action of active and passive forces. Figure 11 displays the corresponding *in vitro* measured active forces shown as solid lines and the *in silico* predicted active forces displayed as squares. With these parameters given, we can now perform a hypothetic computational study to predict the impact of acute and chronic myocardial infarction on the overall force generation.

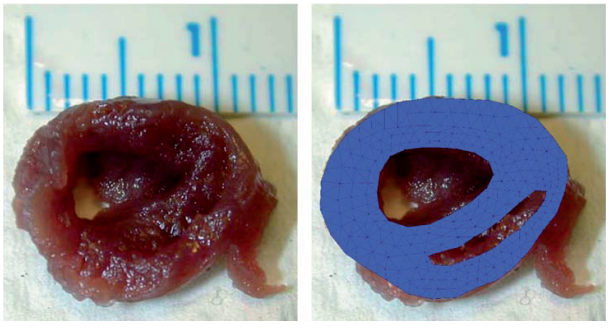

FIG. 8: Representative slice of explanted rat heart **(left)** and finite element discretization **(right)**. The outer diameter of the heart is ∼12 mm, the left ventricular wall thickness is 2.14–2.91 mm, and the slice thickness is 2 mm. In the finite element simulation, fibers are embedded concentrically around the left ventricle.

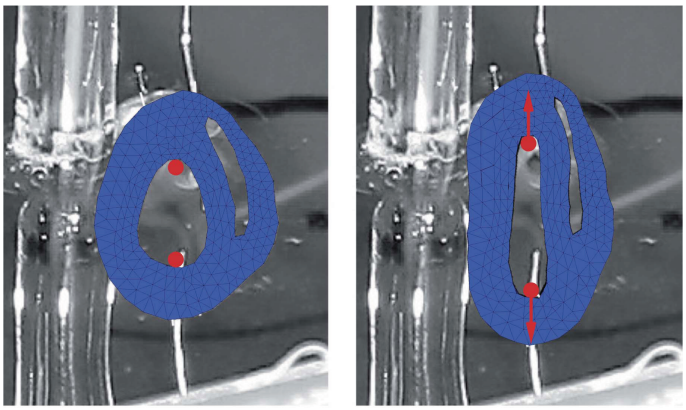

FIG. 9: Mounted undeformed **(left)** and deformed **(right)** heart slice. In the experimental setup, the left ventricle is mounted on two hooks attached to the force transducer. When mounting the slice, it is stretched by one eighth of its original length. In the finite element simulation, this mounting stretch of 12.5% is applied in a initialization step to generate the mounted geometry from the initial, unloaded slice. This setup allows for the controlled application of arbitrary preload to simulate the Frank-Starling mechanism.

FIG. 10: *In silico* predicted rat heart slice configurations. Mounted reference configuration **(left)** and deformed tissue slice configurations under the action of passive forces F^{pas} **(middle)** and total forces $F = F^{\mathrm{pas}} + F^{\mathrm{act}}$ **(right)**.

4.2 Altered Isometric Force Generation upon Acute Infarction

We will now apply the calibrated active cardiac muscle model to predict alterations in isometric force generation in infarcted heart slices. First, we will explore the short-term effects of myocardial infarction. Acute infarction is modeled by the loss of active contractility in the infarcted region, while the passive elastic parameters remain unchanged. We explore the following three scenarios: (i) variation of infarct area fraction at constant infarct location; (ii) variation of degree of infarction across the wall at constant infarct location; and (iii) variation of infarct location at constant area fraction. To simplify the model, we idealize the tissue slice as a thick-walled cylinder with outer and inner radius of $r^{\mathrm{out}} = 10.5$ mm and $r^{\mathrm{inn}} = 3.2$ mm, respectively. The global response of this simplified cylindrical geometry is quantitatively similar to the real rat heart slice displayed in Fig. 11, yet it will be easier to parametrize in terms of infarcted area fractions.

Similar to the previous example, the slice is 2 mm thick, discretized with 16,313 linear tetrahedral finite elements. Guided by our *in vitro* experiment, the passive material parameters are $\nu^{\mathrm{col}} = 1.0 \times 10^8$, $A^{\mathrm{mod}} = 1.0$, $n = 9.5$, $N^{\mathrm{col}} = 2.47 \times 10^9$ mm^{-3}, and $K = 10^7$ N/mm^2. The corresponding active material parameters are $\nu^{\mathrm{fib}} = 13.31$,

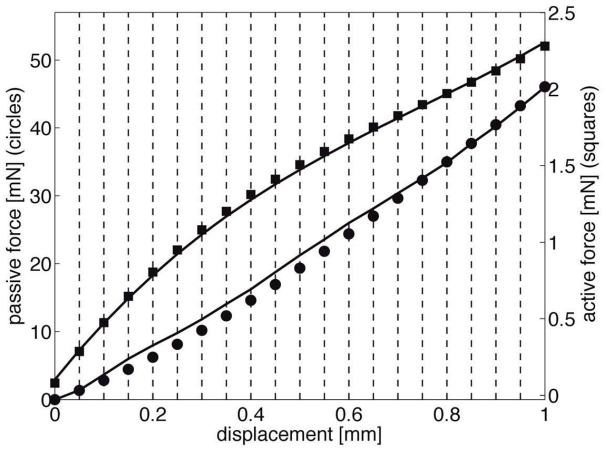

FIG. 11: *In silico* predicted isometric contraction of rat heart slice for different preload levels. Passive force F^{pas} (circles) and the active force F^{act} (squares) are shown for each load step of 0.05 mm. Discrete circles and squares represent the *in silico* predicted values, continuous lines indicate the least-squares fit of the *in vitro* measurements. At maximum preload of ∼15% stretch, the passive force F^{pas} is ∼20 times larger than the active force F^{act}.

$N^{\mathrm{fib}} = 44.1$ mm^{-2}, $f_0 = 1.0 \times 10^{-4}$ mN, $k = 3.0 \times 10^{-4}$ mN, and $\eta = 0.8$. Figure 12 shows the impact of the infarct area fraction on the overall force generation. In this setup, the infarcted area and the healthy tissue are assumed to act in parallel, with the infarct area fraction increasing gradually from 0 to 50%. As expected, as the infarct area fraction increases, the total force $F = F^{\mathrm{pas}} + F^{\mathrm{act}}$ decreases gradually down to $\sim 88\%$ of its maximum value at an infarct area fraction of 50%.

In a second scenario, we explore the gradual increase of the infarct thickness across the ventricular wall. Myocardial infarction is caused by the loss of blood supply, which is provided from the outer ventricular wall. At the event of infarction, cells at the inner wall tend to be affected first and cell death progresses gradually from the inside to the outside of the wall. Figure 13 illustrates the impact of the infarct thickness on the overall force generation, with the infarct thickness increasing gradually from 0 to 100% at a constant infarct area fraction is 30%. As expected, as the infarct thickness increases, the total force $F = F^{\mathrm{pas}} + F^{\mathrm{act}}$ decreases gradually down to 92%, which corresponds to the 30% area fraction reading of the previous example in Fig. 12.

Finally, Fig. 14 displays the influence of the position of the infarct. Because of our particular experimental setup, which circumvents a complicated mounting of a block-type specimen, our test system can only measure uniaxial force generation in one direction. It thus seems natural to explore the difference of the infarct and the remaining tissue acting in parallel versus acting in series. Figure 14 illustrates the difference of these two mounting scenarios. Again, following intuition, the serial setup shows a lower overall force than the parallel setup. For the infarct and the remaining healthy tissue acting in series, the overall tissue force $F = F^{\mathrm{pas}} + F^{\mathrm{act}}$ is 6% lower than for the parallel setup.

4.3 Altered Isometric Force Generation upon Chronic Infarction

In this section, we will explore the long-term effects of myocardial infarction on active force generation. Chronic infarction is modeled by the loss of active contractility, as described in Section 4.2 and the replacement of the soft muscular tissue by stiff scar. To this end, the passive stiffness is increased by increasing the parameter ν^{col} tenfold, while the slice geometry and its finite element discretization remain similar to the previous example. Again, we explore the following two scenarios: (i) variation of infarct area fraction at constant infarct location and (ii) variation of degree of infarction across the wall at constant infarct location. Figure 15 illustrates the chronic alterations in myocardial force generation. In contrast to acute changes in force generation, for the chronic case, the overall force

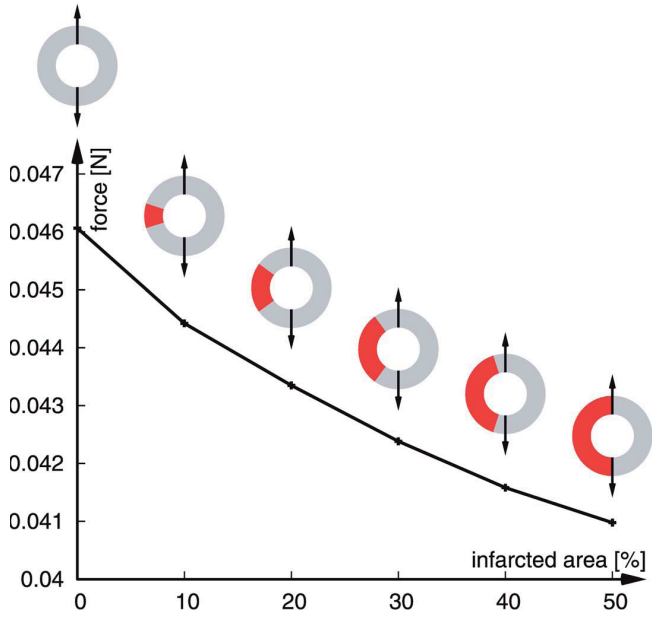

FIG. 12: *In silico* predicted acute force alterations upon myocardial infarction with varying infarct area fraction across the entire wall thickness. Healthy and infarcted tissue are acting in parallel. The infarcted area is increased successively from 0 to 50%. The total force $F = F^{\mathrm{pas}} + F^{\mathrm{act}}$ decreases down to 12% at an infarct area fraction of 50%.

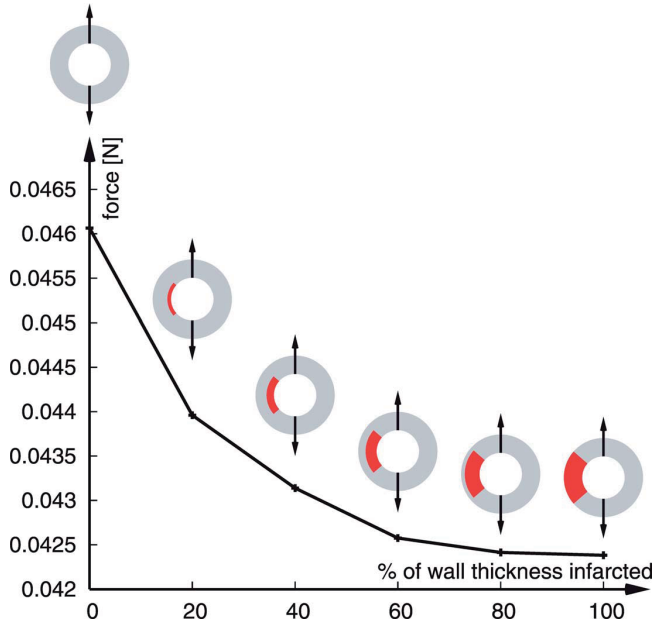

FIG. 13: *In silico* predicted acute force alterations upon myocardial infarction with varying infarct thickness at constant infarct location. Healthy and infarcted tissue are acting in parallel. The infarcted area is increased successively by increasing the infarct thickness from the inside toward the outside. The total force $F = F^{\mathrm{pas}} + F^{\mathrm{act}}$ decreases down to 8% as the infarct affects the entire ventricular wall.

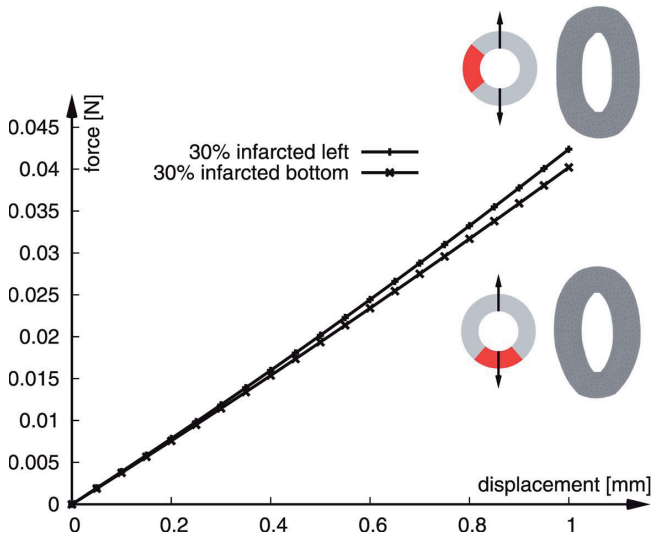

FIG. 14: *In silico* predicted acute force alterations upon myocardial infarction with varying infarct location at constant infarct area of 30% and constant infarct thickness. Healthy and infarcted tissue are acting in parallel (upper curve) and in series (lower curve). The infarcted area is constant at 30%. The total force $F = F^{\text{pas}} + F^{\text{act}}$ of the serial setup is 94% of the force of the parallel setup.

now increases. As the infarct area fraction increases from 0 to 50%, the overall force increases gradually by $\sim 26\%$. For the chronic case, actively contracting tissue has been replaced by stiff scar. Accordingly, the overall force required to obtain the same cardiac output increases.

Last, Fig. 16 documents the chronic changes after myocardial infarction for an infarct thickness gradually increasing from 0 to 100%. This scenario mimics infarcts of different degree, starting at the inner wall and gradually affecting more and more tissue across the thickness as the time of limited blood supply increases. Again, although the tissue becomes weaker in the acute study, the chronic study reveals a gradual stiffening of the tissue slice. The final reading of $F = 0.0507$ N at 100% infarction corresponds to the 30% infarct area fraction reading in Fig. 15.

5. DISCUSSION

Stem cell injection therapies are currently being recognized as a highly promising methodology for cardiac repair after myocardial infarction. Although the *in vivo* probing of different therapeutic parameters, e.g., injection site, amount of cells, or injection time, remains challenging in small and large animals, computational modeling seems to be a reasonable first step to optimize process parameters through systematic *in silico* parameter studies (Wall et al., 2006). To better understand stem cell injection therapies in cardiac disease, current research aims at monitoring and improving cell survival. The functional integration of cells, however, is largely understudied (Abilez et al., 2011), most probably because of the difficulty of defining a reproducible testing environment (Pillekamp et al., 2007b).

In this paper, we introduce a unique test bed to quantify both passive and active force generation in cardiac tissue slices *in vitro*. Avoiding difficulties associated with mounting tissue samples into standard tension test devices, the proposed approach is based on hooking tissue slices into an isometric force measurement device. Recent reports have demonstrated that explanted heart slices remain viable up to three months in long-term culture, displaying spontaneous contraction at their intrinsic rate (Habeler et al., 2009).

Heart slices have therefore been recognized by various research groups as an excellent *in vitro* model system for long-term assessment of disease and experimental therapeutics (Gandolfi et al., 1995; Halbach et al., 2006; Pillekamp et al., 2005, 2007b). Tissue slice experiments are easily reproducible and enable the precise quantification of isometric

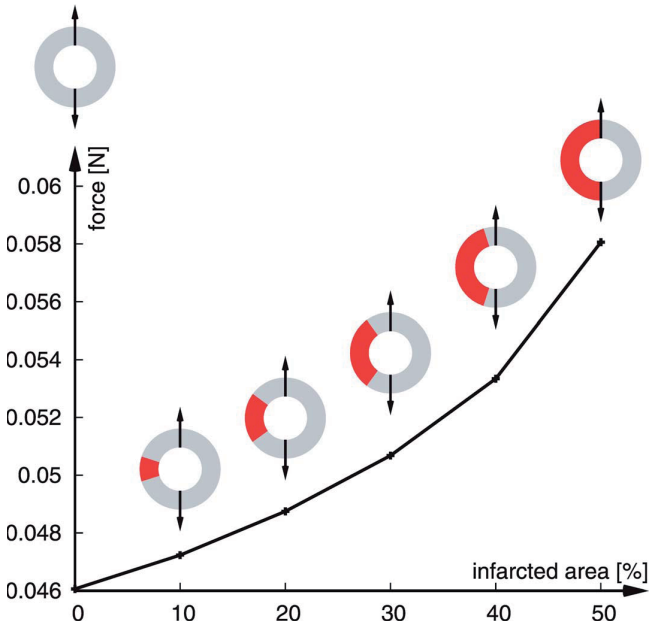

FIG. 15: *In silico* predicted chronic force alterations upon myocardial infarction with varying infarct area fraction across the entire wall thickness. The infarcted area is increased successively from 0 to 50%. The total forces increases by 26% at an infarct area fraction of 50%.

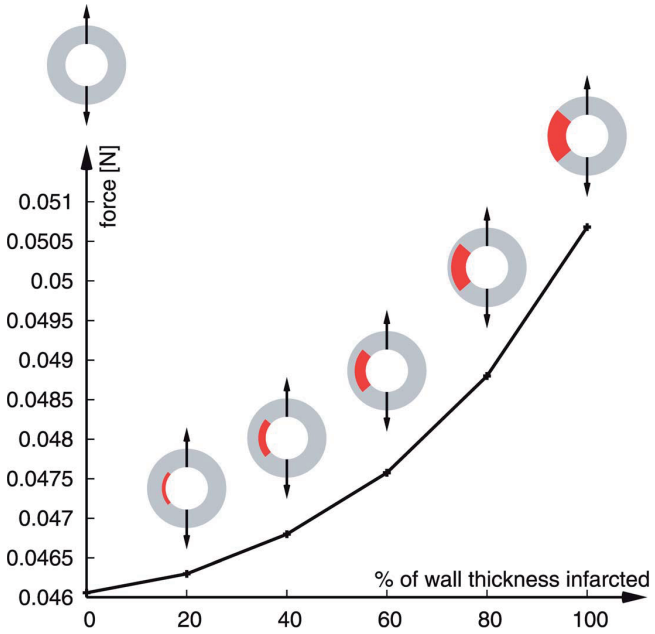

FIG. 16: *In silico* predicted chronic force alterations upon myocardial infarction with varying infarct thickness at constant infarct location. Healthy and infarcted tissue are acting in parallel. The infarcted area is increased successively by increasing the infarct thickness from the inside toward the outside. The total forces increases by 10% as the infarct affects the entire ventricular wall.

force generation in healthy, diseased, and stem cell treated hearts (Habeler et al., 2009; Pillekamp et al., 2007a). As a proof of concept, we have demonstrated the measurement of passive and active forces in healthy rat heart slices at different preload levels. The results are in excellent agreement with recent experiments reported in the literature (Pillekamp et al., 2007a).

Using the measured tissue slice forces, we have calibrated a finite element model of the slice to determine its passive and active material parameter values. Passive forces have been attributed to the surrounding tissue while active forces have been generated by uniaxially contracting muscle fibers (Böl and Reese, 2009; Böl, 2012). Calibrating the model with the measured force-length relation of actively contracting cardiac muscle fibers has allowed us to explore the structure-function relation in axial cardiac tissue slices *in silico*. Motivated by studies reported in the literature (Pillekamp et al., 2007a), we have then applied the model to virtually probe alterations in cardiac force generation in response to myocardial infarction. In particular, we have explored different infarction sites and infarct area fractions, both acutely and chronically. We are now planning to perform rat infarct experiments to evaluate the predictive capacity of the model by comparing the *in silico* predicted active and passive forces with the corresponding *in vitro* measured force profiles.

A potential limitation of our study is the negligence of rate effects, especially given the high *in vivo* heart frequencies. For simplification, our model does neither account for the viscosity of in passive response nor for the force-velocity dependence of the active response. Another limitation is the assumption that the muscle fibers are primarily oriented in the circumferential direction. Conceptually, however, changing the fiber orientation in the model is relatively straightforward once the appropriate fiber directions are known. Determining the exact fiber orientation via tissue histology is part of our current research activities. Because the study reported in this paper is designed as a feasibility study, we have only analyzed six rat heart slices from three different rats and reported one representative force-time curve. We are currently increasing the number of samples to increase the reliability of our database and study statistic deviations. In addition, we are performing tests on axial, longitudinal, and sagittal slices, which taken together, will provide a fully three-dimensional database. This will then allow us to calibrate the active part of the model for physiologically positioned three-dimensional fiber orientations and to refine the passive part using a truly anisotropic more physiological baseline characterization for passive cardiac tissue (Göktepe et al., 2011; Holzapfel and Ogden, 2009).

To date, isometric force generation has primarily been studied in isolated skeletal muscle (Gordon et al., 1966), papillary muscle (Brooks and Conrad, 1999; Capasso et al., 1986; Pollack and Huntsman, 1974), and right and left ventricular trabeculae carneae (Mulieri et al., 1989; Pollack and Huntsman, 1974), presumably because they are all unidirectional, highly structured, and relatively easy to isolate. When testing isolated muscle fibers in their physiological stretch range, the active force component is much larger than the passive force. Our studies, however, confirmed a previously reported much lower active-to-passive force ratio for slices of cardiac muscle tissue (Pillekamp et al., 2007a). With the help of a systematic series of experiments, we are currently exploring the role of dissection injury as potential cause for active force reduction and passive force increase. In addition, we are analyzing the degrees of hypoxia and cell death by investigating whether the active and passive force generation scale linearly with slice thickness (Mulieri et al., 1989) and by evaluating for histological evidence of apoptosis and necrosis. However, we do not expect to find significant tissue damage, because it has been demonstrated that sliced heart structures remain intact and functional without induction of apoptosis at least 48 h postexplantation (Pillekamp et al., 2007b).

Another interesting feature that can be probed easily with the current test setup is the correlation between active muscle force and stimulation frequency (Pillekamp et al., 2007b). Through systematic studies at different excitation rates, we seek to justify our activation at 1 Hz, which is below the *in vivo* frequency of rat hearts of approximately 5–8 Hz, but well above the intrinsic *in vitro* frequency of ~ 0.5 Hz (Habeler et al., 2009).

An interesting side aspect of the proposed model system is that we can not only acquire total, passive, and active forces, but also quantify muscle force adaptation times. Adaptation in the form of adjustment to a new preload level is important in everyday life, and fast adaptation ensures that the heart is capable of adjusting its pump function to an increased or decreased stroke volume. In this paper, we have focused exclusively on the converged passive and active forces, but we plan to explore the rate of convergence (i.e., the adaptation time) in future disease-related studies.

Despite these limitations, we believe that ventricular slices in culture provide a powerful multicellular *in vitro*/*in silico* model system suitable to explore active force generation in healthy, infarcted, and stem cell treated hearts.

For example, an exciting finding of the present study is that restoration of cardiac function may greatly benefit from removing stiff scar tissue before even considering to supplement a failing heart with passive or active structural support. Motivated by the idea to reliably predict active cardiac force generation, we are currently using the proposed model system to systematically optimize different process parameters for stem cell-based cardiac repair.

ACKNOWLEDGMENTS

The material of this paper is based on work supported by the National Science Foundation CAREER Award No. CMMI-0952021, "The Virtual Heart–Exploring the Structure-Function Relationship in Electroactive Cardiac Tissue," by the National Science Foundation ERFI program through Grant No. EFRI-CBE-0735551 "Engineering of Cardiovascular Cellular Interfaces and Tissue Constructs", by the National Institutes of Health under Grant No. HL089027 "Nanostructuring and Molecular Imaging of Engineered Cardiovascular Tissue," by the California Institute for Regenerative Medicine under Grant No. RC1-00151-1 "Engineering a cardiovascular tissue graft from human embryonic stem cells."

REFERENCES

Abilez, O., Benharash, P., Miyamoto, E., Gale, A., Xu, C., Zarins, C. K., P19 progenitor cells progress to organized contracting myocytes after chemical and electrical stimulation: Implications for vascular tissue engineering, *J. Endovasc. Ther.*, vol. **13**, no. 3, pp. 377–388, 2006a.

Abilez, O., Benharash, P., Mehrotra, M., Miyamoto, E., Gale, A., Picquet, J., Xu, C., and Zarins, C., A novel culture system shows that stem cells can be grown in 3D and under physiologic pulsatile conditions for tissue engineering of vascular grafts, *J. Surg. Res.*, vol. **132**, no. 2, pp. 170–178, 2006b.

Abilez, O. J., Wong, J., Prakash, R., Deisseroth, K., Zarins, C. K., and Kuhl, E., Multiscale computational models for optogenetic control of cardiac function, *Biophys. J.*, vol. **101**, no. 4, pp. 1326–1334, 2011.

Allen, D. G., Jewell, B. R., and Murray, J. W., The contribution of activation processes to the length-tension relation of cardiac muscle, *Nature*, vol. **248**, no. 449, pp. 606–607, 1974.

Berne, R. M. and Levy, M. N., *Cardiovascular Physiology*, The Mosby Monograph Series, Mosby, St. Louis, 2001.

Bers, D. M., *Excitation-Contraction Coupling and Cardiac Contractile Force*, Springer, New York, 2001.

Böl, M. and Reese, S., Finite element modelling of rubber-like polymers based on chain statistics, *Int. J. Solid Struct.*, vol. **43**, pp. 2–26, 2006.

Böl, M. and Reese, S., A new approach for the simulation of skeletal muscles using the tool of statistical mechanics, *Mat. Sci. Eng. Tech.*, vol. **38**, no. 12, pp. 955–964, 2007.

Böl, M. and Reese, S., Micromechanical modelling of skeletal muscles based on the finite element method, *Comput. Methods Biomech. Biomed. Eng.*, vol. **11**, no. 5, pp. 489–504, 2008.

Böl, M., Reese, S., Parker, K. K., and Kuhl, E., Computational modeling of muscular thin films for cardiac repair, *Comput. Mech.*, vol. **43**, pp. 535–544, 2009.

Böl, M., Micromechanical modelling of skeletal muscles: From the single fibre to the whole muscle, *Arch. Appl. Mech.*, vol. **80**, pp. 557–567, 2012.

Brooks, W. W. and Conrad, C. H., Differences between mouse and rat myocardial contractile responsiveness to calcium, *Comput. Biochem. Physiol. A*, vol. **124**, no. 2, pp. 139–147, 1999.

Bustamante, C., Marko, J. F., Siggia, E. D., and Smith, S., Entropic elasticity of lambda-phage DNA, *Science*, vol. **265**, no. 5178, pp. 1599–1600, 1994.

Capasso, J. M., Malhotra, A., Scheuer, J., and Sonnenblick, E. H., Myocardial biochemical, contractile, and electrical performance after imposition of hypertension in young and old rats, *Circ. Res.*, vol. **58**, no. 4, pp. 445–460, 1986.

Costa, K. D., Holmes, J. W., and McCulloch, A. D., Modelling cardiac mechanical properties in three dimensions, *Phil. Trans. R. Soc. Lond. A*, vol. **359**, no. 1783, pp. 1233–1250, 2001.

Dokos, S., Smaill, B. H., Young, A. A., and LeGrice, I. J., Shear properties of passive ventricular myocardium, *Am. J. Physiol. Heart Circ. Physiol.*, vol. **283**, pp. H2650–2659, 2002.

Ehret, A. E. and Itskov, M., Modeling of anisotropic softening phenomena: Application to soft biological tissues, *Int. J. Plast.*, vol. **25**, pp. 901–919, 2009.

Flory, P. J., *Statistical Mechanics of Chain Molecules*, Wiley, Hoboken, NJ, 1969.

Ganong, W. F., *Review of Medical Physiology*, McGraw-Hill/Appleton & Lange, New York, 2003.

Gandolfi, A. J., Brendel, K., Fisher, R. L., and Michaud, J. P., Use of tissue slices in chemical mixture tosicology and interspecies investigations, *Toxicology*, vol. **105**, pp. 285–290, 1995.

Göktepe, S. and Kuhl, E., Computational modeling of electrophysiology: A novel finite element approach, *Int. J. Numer. Methods Eng.*, vol. **79**, pp. 156–178, 2009.

Göktepe, S. and Kuhl, E., Electromechanics of the heart–A unified approach to the strongly coupled excitation-contraction problem, *Comput. Mech.*, vol. **45**, pp. 227–243, 2010.

Göktepe, S., Acharya, S. N. S., Wong, J., and Kuhl, E., Computational modeling of passive myocardium, *Int. J. Numer. Methods Biomed. Eng.*, vol. **27**, pp. 1–12, 2011.

Göktepe, S., Abilez, O. J., and Kuhl, E., A generic approach towards finite growth with examples of athlete's heart, cardiac dilation, and cardiac wall thickening, *J. Mech. Phys. Solids*, vol. **58**, pp. 1661–1680, 2010a.

Göktepe, S., Abilez, O. J., Parker, K. K., and Kuhl, E., A multiscale model for eccentric and concentric cardiac growth through sarcomerogenesis, *J. Theor. Bio*, vol. **265**, pp. 433–442, 2010b.

Gordon, A. M., Huxley, A. F., and Julian, F. J., The variation in isometric tension with sarcomere length in vertebrate muscle fibres, *J. Physiol.*, vol. **184**, no. 1, pp. 170–192, 1966.

Habeler, W., Pouillot, S., Plancheron, A., Puceat, M., Peschanski, M., and Monville, C., An *in vitro* beating heart model for long-term assessment of experimental therapeutics, *Cardiovasc. Res.*, vol. **81**, pp. 253–259, 2009.

Halbach, M., Pillekamp, F., Brockmeier, K., Hescheler, J., Muller-Ehmsen, J., and Reppel, M., Ventricular slices of adult mouse hearts–A new multicellular *in vitro* model for electrophysiological studies, *Cell Phys. Biochem.*, vol. **18**, pp. 1–8, 2006.

Holzapfel, G. A. and Ogden, R. W., Constitutive modelling of passive myocardium. A structurally-based framework for material characterization, *Phil. Trans. R. Soc. London A*, vol. **367**, pp. 3445–3475, 2009.

Hunter, P. J., McCulloch, A. D., and ter Keurs, H. E., Modelling the mechanical properties of cardiac muscle, *Prog. Biophys. Mol. Biol.*, vol. **69**, no. 2–3, pp. 289–331, 1998.

Huxley, H. and Hanson, J., Changes in the cross-striations of muscle during contraction and stretch and their structural interpretation, *Nature*, vol. **173**, no. 4412, pp. 973–976, 1954.

Itoh, A., Krishnamurthy, G., Swanson, J., Ennis, D., Bothe, W., Kuhl, E., Karlsson, M., Davis, L., Miller, D. C., and Ingels, N. B., Active stiffening of mitral valve leaflets in the beating heart, *Am. J. Physiol. Heart Circ. Physiol.*, vol. **296**, pp. 1766–1773, 2009.

Kotikanyadanam, M., Göktepe, S., and Kuhl, E., Computational modeling of electrocardiograms–A finite element approach towards cardiac excitation, *Int. J. Numer. Methods Biomed. Eng.*, vol. **26**, pp. 524–533, 2010.

Kratky, O. and Porod, G., Röntgenuntersuchung gelöster Fadenmoleküle, *Recueil*, vol. **68**, pp. 1106–1122, 1949.

Kuhl, E., Garikipati, K., Arruda, E. M., and Grosh, K., Remodeling of biological tissue–Mechanically induced reorientation of a transversely isotropic chain network, *J. Mech. Phys. Solids*, vol. **53**, no. 7, pp. 1552–1573, 2005.

Kuhl, E., Menzel, A., and Garikipati, K., On the convexity of transversely isotropic chain network models, *Phil. Mag.*, vol. **86**, no. 21–22, pp. 3241–3258, 2006.

Kuhl, E. and Holzapfel, G. A., A continuum model for remodeling in living structures, *J. Mat. Sci.*, vol. **42**, pp. 8811–8823, 2007.

Kumar, V., Abbas, A. K., and Fausto, N., *Robbins and Cotran Pathologic Basis of Disease*, Elsevier Saunders, Philadelphia, 2005.

Mulieri, L. A., Hasenfuss, G., Ittleman, F., Blanchard, E. M., and Alpert, N. R., Protection of human left ventricular myocardium from cutting injury with 2.3/butanedione monoxime, *Circ. Res.*, vol. **65**, pp. 1441–1449, 1989.

Omens, J. H., MacKenna, D. A., and McCulloch, A. D., Measurements of strain and analysis of stress in resting rat left ventricular myocardium, *J. Biomech.*, vol. **26**, no. 6, pp. 665–676, 1993.

Opie, L. H., *Heart Physiology: From Cell to Circulation*, Lippincott Williams & Wilkins, Philadelphia, 2003.

Pillekamp, F., Reppel, M., Dinkelacker, V., Duan, Y., Jazmati, N., Bloch, W., Brockmeier, K., Hescheler, J., Fleischmann, B. K., and Koehling, R., Establishment and characterization of a mouse embryonic heart slice preparation, *Cell Physiol. Biochem.*, vol.

16, no. 1-3, pp. 127–132, 2005.

Pillekamp, F., Reppel, M., Rubenchyk, O., Pfannkuche, K., Matzkies, M., Bloch, W., Sreeram, N., Brockmeier, K., and Hescheler, J., Force measurements of human embryonic stem cell-derived cardiomyocytes in an in vitro transplantation model, *Stem Cells*, vol. **25**, no. 1, pp. 174–180, 2007a.

Pillekamp, F., Halbach, M., Reppel, M., Rubenchyk, O., Pfannkuche, K., Xi, J. Y., Bloch, W., Sreeram, N., Brockmeier, K., and Hescheler, J., Neonatal murine heart slices. A robust model to study ventricular isometric contractions, *Physiol. Biochem.*, vol. **20**, pp. 837–846, 2007.

Pollack, G. H. and Huntsman, L. L., Sarcomere length-active force relation in living mammalian cardiac muscle, *Am. J. Physiol.*, vol. **227**, pp. 383–389, 1974.

Schmid, H., Nash, M. P., Young, A. A., and Hunter, P. J., Myocardial material parameter estimation–A comparative study for simple shear, *J. Biomech. Eng.*, vol. **128**, pp. 742–750, 2006.

Schmid, H., O'Callaghan, P., Nash, M. P., Lin, W., LeGrice, I. J., Smaill, B. H., Young, A. A., and Hunter, P. J., Myocardial material parameter estimation–A non-homogeneous finite element study from simple shear tests, *Biomech. Model Mechanobio*, vol. **7**, pp. 161–173, 2008.

Schmid, H., Wang, Y. K., Ashton, J., Ehret, A. E., Krittian, S. B. S., Nash, M. P., and Hunter, P. J., Myocardial material parameter estimation–A comparison of invariant based orthotropic constitutive equations, *Comput. Methods Biomech. Biomed. Eng.*, vol. **12**, pp. 283–295, 2009.

Siebert, T., Rode, C., Herzog, W., Till, O., and Blickhan, R., Nonlinearities make a difference: Comparison of two common Hill-type models with real muscle, *Biol. Cybern.*, vol. **98**, pp. 133–143, 2008.

Treloar, L. R. G., *The Physics of Rubber Elasticity*, Clarendon Press, Oxford, 1975.

Tsamis, A., Bothe, W., Kvitting, J. P., Swanson, J. C., Miller, D. C., and Kuhl, E., Active contraction of cardiac muscle: *In vivo* characterization of mechanical activation sequences in the beating heart, *J. Mech. Behavior Biomed. Mater.*, vol. **4**, pp. 1167–1176, 2011.

Wall, S. T., Walker, J. C., Healy, K. E., Ratcliffe, M. B., and Guccione, J. M., Theoretical impact of the injection of material into the myocardium: A finite element model simulation, *Circulation*, vol. **114**, no. 24, pp. 2627–2635, 2006.

Wollert, K. C., Meyer, G. P., Lotz, J., Ringes-Lichtenberg, S., Lippolt, P., Breidenbach, C., Fichtner, S., Korte, T., Hornig, B., Messinger, D., Arseniev, L., Hertenstein, B., Ganser, A., and Drexler, H., Intracoronary autologous bone-marrow cell transfer after myocardial infarction: The BOOST randomised controlled clinical trial, *Lancet*, vol. **364**, no. 9429, pp. 141–148, 2004.

Zimmermann, W. H., Didié, M., Döker, S., Melnychenko, I., Naito, H., Rogge, C., Tiburcy, M., and Eschenhagen, T., Heart muscle engineering: An update on cardiac muscle replacement therapy, *Cardiovasc. Res.*, vol. **71**, no. 3, pp. 419–429, 2006.